9

Aspects of volcanic hazards assessment for the Bataan nuclear power plant, Luzon Peninsula, Philippines

A. C. M. Volentik, C. B. Connor, L. J. Connor, C. Bonadonna

How would the eruption of a volcano affect a nearby nuclear power plant (NPP)? Specifically, would the products of a volcanic eruption impact the operation of a NPP located near an erupting volcano? The answer to this question begins with an assessment of the geological phenomena that result from volcanic eruptions. These phenomena are diverse, and include tephra fallout, pyroclastic flows and lahars, among others (Connor *et al.*, Chapter 3, this volume). The effects of these phenomena depend on a host of factors, such as the proximity of the volcano to the NPP, the size and character of the eruption, wind direction, and topography around the volcano.

The complexity and uncertainty associated with these phenomena suggest that their potential impacts be assessed probabilistically. One important aspect of probabilistic assessment involves forecasting the timing of eruptions. When will the next eruption occur? Or, phrased another way, how much time must elapse before a volcano no longer has a credible potential for future eruptions? This question is not easily resolved, as volcanoes may go thousands of years, or even tens of thousands of years without erupting. A second aspect of volcanic hazard assessment is estimation of the effects of volcanic eruptions, once they occur. Which areas might be inundated by lahars, or experience tephra fallout? As eruption magnitudes and their effects vary widely, this question must also be answered probabilistically. Admittedly, assessment of the timing and consequences of potential eruptions is a daunting task, requiring site-specific data, a refined understanding of volcanic processes, and computational tools to actually estimate probabilities.

In the face of these complexities, a systematic approach is warranted. Hill *et al.* (Chapter 25, this volume), recommend guidelines for volcanic hazard assessment for surface nuclear facilities that provide a systematic approach. In this chapter these recommended guidelines are applied to a specific NPP site located in the Philippines. Our goal is to illustrate key points of the application of the recommended guidelines to volcanic hazard assessment for surface nuclear facilities.

We illustrate aspects of volcanic hazard assessment using the Bataan nuclear power plant (BNPP) site, located on Napot Point on the west coast of the Bataan Peninsula, Western Luzon Peninsula, Philippines, at 14°38′ N, 120°19′ E, or, in UTM Zone 51 N coordinates, 210 500 E, 1 619 000 N (Figure 9.1). This NPP was sited and constructed during the late 1970s and early 1980s, using then current designs for a pressurized water reactor. Although some nuclear fuel was delivered, the reactor never operated. The project was quite controversial at the time of siting and construction. In the United States, for example, questions arose about whether hazard assessments at the site were partly the responsibility of the US Nuclear Regulatory Commission, because US companies exported technology used to construct the BNPP (D'Amato and Engel, 1988). The US Nuclear Regulatory Commission ultimately decided that it had no legal role in reviewing the hazards assessments for the BNPP. Nevertheless, concerns about the siting assessment for the BNPP remained. The Union of Concerned Scientists cited the proximity of the site to the potentially active Mt. Natib volcano as a major source of concern (D'Amato and Engel, 1988). The conclusions of volcanic hazard assessments performed by a US consulting company (EBASCO, 1977; 1979) on behalf of the Philippine Atomic Energy Commission were questioned by US scientists (Newhall, 1979), experts from the International Atomic Energy Agency (IAEA, 1978) and oversight panels in the Philippines.

It is not our intent to review, or recreate, this controversy. Rather, data gathered during the site investigation and after the site investigation are used to assess hazards, within the guidelines outlined by Hill *et al.* (Chapter 25, this volume), as an illustration of the application of these guidelines. This assessment, some 30 a after construction of the NPP, utilizes modern methods for numerical modeling of volcanic phenomena, particularly with regard to assessment of tephra fallout hazards and susceptibility of the site to pyroclastic flows and lahars. As mentioned previously, this assessment stops short of a comprehensive volcanic hazard assessment. In this regard, one criticism of the original hazard assessment was the lack of adequate geologic mapping of Mt. Natib volcano (IAEA, 1978; Newhall, 1979). To our knowledge, such comprehensive mapping has not yet been undertaken for Mt. Natib volcano and hence a comprehensive hazard assessment, fully meeting the recommendations described by Hill *et al.* (Chapter 25, this volume), is not possible at this time.

9.1 Volcanological setting

The BNPP site is located within a Quaternary volcanic province known as the Bataan Lineament (Wolfe and Self, 1983), formed by the eastward subduction of the South China Sea floor along the Manila Trench off the west coast of Luzon

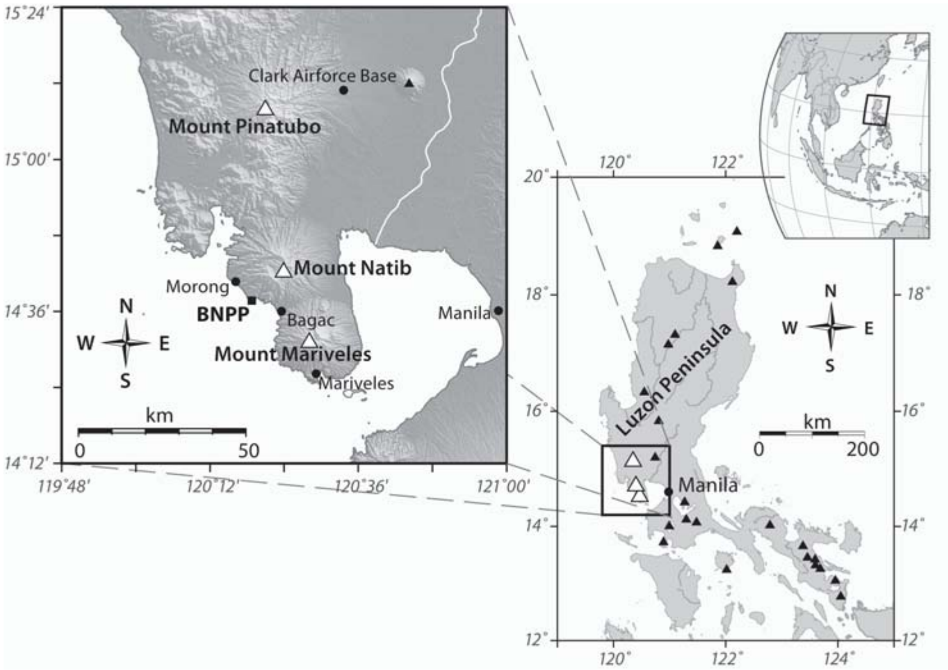

Fig. 9.1. Location map showing the Bataan Peninsula, forming the southern part of the Luzon Peninsula within the Philippines archipelago. Black triangles indicate active volcanoes. White triangles indicate active volcanoes closest to the BNPP. The Bataan Peninsula is formed from 2 volcanoes, Mt. Natib to the north and Mt. Mariveles to the south. The location of the BNPP is marked with a black square (DEM data from CGIAR-CSI, 2004).

Peninsula. The Bataan Lineament is 320 km long and comprises at least 27 volcanoes, including Mt. Natib (Figure 9.1). The summit of Mt. Natib volcano is located about 15 km NE of the BNPP. Mt. Pinatubo and Mt. Mariveles volcanoes, which may be relevant to the hazard assessment, lie about 57 km N and 22 km SE of the site, respectively (Figure 9.1).

Mt. Natib and Mt. Mariveles are both Quaternary composite volcanoes and together form the dominant topographic features of the Bataan Peninsula. These volcanoes have not erupted historically. Geologic mapping and radiometric dating of Mt. Natib deposits indicate that this volcano has produced violent explosive eruptions during the last several hundred thousand years. These eruptions produced tephra fallout, pyroclastic density currents (pyroclastic flows) and secondary lahars (EBASCO, 1977; Newhall, 1979; Wolfe and Self, 1983; Siebert and Simkin, 2007). The Napot Point Tuff, as described by Newhall (1979), is a pyroclastic flow deposit that resulted from such eruptions. The Napot Point Tuff and lahar deposits are located within the BNPP site area. Details of past eruptions are difficult to decipher, however, because both Mt. Natib and Mt. Mariveles volcanoes have poorly defined stratigraphies. Geologic mapping (Newhall, 1979; Ruaya and Panem, 1991) is challenging on the peninsula, in part due to poor exposures in this tropical environment and in part due to complexities of volcanic stratigraphy in an arc terrain.

The volcanic hazard assessment made by EBASCO (1977) preceded the dramatic volcanic eruptions of Mt. Pinatubo in 1991. After dormancy of about 540 a, Mt. Pinatubo reawakened in April 1991. The volcanic activity culminated in an explosive Plinian eruption on 15 June 1991, that produced a strong vertical plume and several pyroclastic density currents (Newhall and Punongbayan, 1996). This eruption is important for hazard assessment at the BNPP in two respects. First, the eruption directly affected the site, depositing ~ 6 cm of tephra in the site area. Second, the Mt. Pinatubo eruption provides an analog for potential future eruptions of Mt. Natib and Mt. Mariveles, at which no historical eruptions have occurred and for which geologic mapping is incomplete.

The 1991 Mt. Pinatubo eruption column reached a maximum height of 35−40 km (Koyaguchi and Tokuno, 1993; Holasek *et al.*, 1996; Koyaguchi, 1996; Paladio-Melosantos *et al.*, 1996; Rosi *et al.*, 2001). Tephra fallout occurred throughout the entire eruption and deposited several layers of pumiceous lapilli and ash, with two distinct tephra layers associated with the climatic eruption (Koyaguchi and Tokuno, 1993; Paladio-Melosantos *et al.*, 1996; Koyaguchi, 1996; Koyaguchi and Ohno, 2001). Voluminous pyroclastic flows were generated during the eruption that traveled as much as 12−16 km radially from the vent and were able to overcome topographic ridges as high as 400 m in proximal areas (Scott *et al.*, 1996). These pyroclastic deposits were remobilized by heavy rainfalls, triggering large lahars around Mt. Pinatubo shortly after and more than six years following the eruption (Rodolfo *et al.*, 1996; Wolfe and Hoblitt, 1996; Daag, 2003; van Westen and Daag, 2005).

Although Mt. Natib and Mt. Mariveles seem to have erupted volcanic products slightly more mafic than Mt. Pinatubo (Defant *et al.*, 1991; Newhall *et al.*, 1996), these volcanoes are similar in several respects. Summit calderas truncate the three edifices. Mt. Natib caldera is 6 × 7 km, Mt. Mariveles caldera is 4 km in diameter and Mt. Pinatubo caldera is the smallest, only 2.5 km in diameter. The caldera of Mt. Pinatubo formed as a result of one collapse event following the 1991 eruption. It is unclear if the calderas on Mt. Natib and Mt. Mariveles were similarly formed following only one explosive eruption or by incremental collapses through time associated with multiple eruptions. At least for Mt. Natib, pyroclastic flows seem to have traveled more than 10 km from the caldera, to a point where they reached the sea, and secondary lahars associated with these pyroclastic flows were generated and traveled in main drainages. No tephra-fall deposits have been reported or mapped for eruptions from Mt. Natib or Mt. Mariveles (EBASCO, 1977; 1979; Newhall, 1979). However, this does not imply that extensive tephra-fall did not accompany past volcanic eruptions from these volcanoes. For comparison, the tephra deposit from the 1991 eruption of Mt. Pinatubo has been almost completely eroded away (Daag, 2003; Newhall, 2007, personal communication).

Today, volcanic activity at Mt. Natib is manifest by thermal springs that are located within the summit caldera (Ruaya and Panem, 1991), suggesting the presence of a hydrothermal system within the volcano. Mt. Natib and Mt. Mariveles are not currently monitored, so nothing more is known about the current state of activity at these volcanoes.

Much of what is known about the history of eruptions at Mt. Natib volcano is based on radiometric age determinations from samples collected by EBASCO (1977), Wolfe and Self (1983), and the Philippine Institute of Volcanology and Seismology (PHIVOLCS). Without adequate stratigraphic constraints, these age determinations can only provide a snapshot of volcanic activity, rather than information about the stratigraphic sequence or variations in the rate of volcanic activity. EBASCO (1977) concluded that Mt. Natib volcano was active between 0.069−1.6 Ma, based on a series of 27 K/Ar dates on lavas and pyroclastic flows exposed on the flanks of the volcano. A total of 31 K/Ar dates reported by Wolfe and Self (1983) suggest a range of activity from 0.54−3.9 Ma. In addition, fission track ages on seven pumice samples range from 20−59 ka, but EBASCO (1977; 1979) suggested these may be underestimates of eruption age due to potential Uranium migration in these samples. In 1999, PHIVOLCS made an uncalibrated ^{14}C age determination of 27 ± 0.63 ka on charcoal within a young pyroclastic flow deposit on the eastern flank of Mt. Natib (written communication, C. Newhall, 1999). More recently, Cabato *et al.* (2005) found evidence to support an even younger explosive eruption on the western flanks of Mt. Natib. Based on a high-resolution seismic study of the Subic Bay, Cabato *et al.* (2005) proposed an age of 11.3−18 ka for a potential pyroclastic deposit interlayered with sediments in the eastern Subic Bay. This pyroclastic deposit is thought to originate from an explosive eruption in the northwestern area of the breached Mt. Natib caldera. These age determinations are much younger than the youngest age of 69 ka reported by EBASCO (1977) in their hazard assessment of Mt. Natib, highlighting that reconnaissance mapping and dating may have missed these younger units on the western side. The occurrence of young pyroclastic flows on the western flanks of the volcano emphasizes the potential for volcanic hazards around Mt. Natib on both the western and eastern flanks (see EBASCOs reports 1977, 1979). Unfortunately, there are no available ages for the Napot Point Tuff, which crops out in the BNPP site vicinity. A reconnaissance suite of radiometric dates have been reported for Mt. Mariveles volcano. Wolfe and Self (1983) reported a range of activity from 0.19−4.1 Ma, based on 20 samples. However, the most recent eruption at Mt. Mariveles may be as young as 2050 BC (uncalibrated ^{14}C date, Siebert and Simkin, 2007).

9.2 Assessment of volcano capability

For the closest volcanoes to the BNPP site, the frequency and timing of past volcanic events are incompletely understood and thus highly uncertain. The concept of a capable volcano (Hill *et al.*, Chapter 25, this volume) is used to assess the potential for Mt. Natib and Mt. Mariveles volcanoes to produce hazardous phenomena that may reach the BNPP. Following its 1991 eruption, Mt. Pinatubo is clearly a capable volcano, as ~ 6 cm of tephra fell on the BNPP during that eruption. As described in detail in Chapter 25, a capable volcano is one for which both (*i*) a future eruption or related volcanic event is credible; and (*ii*) such an event has the potential to produce phenomena that may affect a site. If Mt. Natib or Mt. Mariveles volcanoes are capable, a detailed, site-specific volcanic hazard assessment is warranted that considers the likelihood of occurrence and associated uncertainties for volcanic phenomena that may reach a site.

One step in determining a volcano's capability is to evaluate its potential for future eruptions. Activity documented during the Holocene (i.e. within the last 10 ka) is one criterion used to determine that a volcano appears capable of future volcanic eruptions (e.g. Hill *et al.*, Chapter 25, this volume). There is no definitive evidence that Mt. Natib or Mt. Mariveles volcanoes have erupted during the Holocene. Nevertheless, determining Holocene eruptive activity is difficult, especially in the tropical environment of these volcanoes and where mapping is incomplete. In such cases evidence of current volcanic activity includes ongoing volcanic unrest, or the presence of an active hydrothermal system and related phenomena. As Mt. Natib and Mt. Mariveles volcanoes are not monitored, there is no information available regarding current unrest, such as the occurrence of volcano-tectonic earthquakes or ground deformation. However, the presence of thermal springs within Mt. Natib's caldera (Ruaya and Panem, 1991) is indicative of an active hydrothermal system. Thus, future eruptions of Mt. Natib are possible (c.f. Siebert and Simkin, 2007). Therefore, an analysis should be made to assess the possibility of volcanic phenomena reaching the site of the BNPP, given a potential eruption of Mt. Natib volcano. Hydrothermal activity has not been reported at Mt. Mariveles volcano, but, as previously noted, one ^{14}C date suggests that Holocene activity has occurred. Thus Mt. Mariveles volcano may also be a capable volcano, based on the timing of past eruptions.

The probability of future eruptions of Mt. Natib is highly uncertain, given the incomplete record of radiometric age determinations and lack of detailed stratigraphic control on important geologic units. Based on this incomplete record, EBASCO (1977) estimated the probability of a future volcanic eruption of Mt. Natib volcano to be $\sim 3 \times 10^{-5}\,\mathrm{a}^{-1}$. The global record of repose intervals preceding large Plinian eruptions (i.e. Volcano Explosivity Index (VEI) 6–7) of long-dormant volcanoes (Siebert and Simkin, 2007) provides one means of evaluating this probability. Connor *et al.* (2006) found that repose intervals preceding VEI 6–7 eruptions of long-dormant volcanoes follow a log-logistic probability distribution. Applying this probability model and using a repose interval of 14.65 ka, based on the averaged date of the youngest known pyroclastic flow (11.3–18 ka) on Mt. Natib (Cabato et al., 2005), the probability of a VEI 6–7 eruption of Mt. Natib is $\approx 1 \times 10^{-4} - 2 \times 10^{-4}\,\mathrm{a}^{-1}$, with 95% confidence, which is almost one order of magnitude greater than the EBASCO (1977) result. Such probabilities appear sufficient to consider future eruptions as credible events, and indicate that a hazard analysis for these eruptions appears warranted (Hill *et al.*, Chapter 25, this volume). Following the same approach but using a repose interval of 4.05 ka, based on the youngest date on volcanic products from Mt. Mariveles, the probability of a VEI 6–7 eruption of Mt. Mariveles is $\approx 3.5 \times 10^{-4} - 6 \times 10^{-4}\,\mathrm{a}^{-1}$, with 95% confidence.

Had we applied this probabilistic method in 1990, before the eruption of Mt. Pinatubo, the probability of a VEI 6-7 eruption of Mt. Pinatubo would have been $\approx 0.6 \times 10^{-3} - 1 \times 10^{-3}\,\mathrm{a}^{-1}$, using a repose interval of 0.54 ka based on its most recent known explosive eruption prior to 1991. Repose intervals between eruptive episodes for the most recent eruptions of Mt. Pinatubo (Newhall *et al.*, 1996), not including the 1991 eruption, are chronologically: 2.5 ka, 2.5 ka, 3.5 ka, 8.4 ka and 17.6 ka (Newhall *et al.*, 1996; Siebert and Simkin, 2007). Assuming that the timing of eruptions is described by a Poisson process (Connor *et al.*, Chapter 3, this volume), the interval estimate of repose for Mt. Pinatubo is 3.4–21.2 ka, with 95% confidence. This interval corresponds to a probability of an eruption of Mt. Pinatubo to be $0.5 \times 10^{-4} - 3 \times 10^{-4}\,\mathrm{a}^{-1}$. A bootstrap with replacement procedure (Efron and Tibshirani, 1991) yields an interval estimate of 3.8–9.9 ka, with 95% confidence, corresponding to a probability of an eruption of Mt. Pinatubo of $1 \times 10^{-4} - 2.6 \times 10^{-4}\,\mathrm{a}^{-1}$. Note that the period between eruptions of Mt. Pinatubo becomes shorter with time. This may reflect nonstationarity in repose intervals between eruptions, or may simply reflect sampling bias, due to difficulty in distinguishing eruptive units in the older stratigraphic record. Regardless, it appears that the probability of eruptions of Mt. Pinatubo, prior to the 1991 eruptions, were $\sim 1-2$ orders of magnitude greater than probabilities of large explosive eruptions currently estimated for Mt. Natib. Our interpretation of this comparison is that, although the probability of an explosive eruption of Mt. Natib appears to be much lower than the probability of eruptions of Mt. Pinatubo, explosive eruptions of Mt. Natib are credible.

For Mt. Natib volcano, evidence of an active hydrothermal system, and probability estimates, both indicate that the volcano has a credible potential for future eruptions. The potential for volcanic phenomena to impact the BNPP site should be estimated. This step is accomplished by estimating screening distance values for volcanic phenomena, such as tephra fallout, lahars, and pyroclastic flows, that have the highest potential to affect the BNPP site, adversely. These screening distance values consider the potential for volcanic phenomena to reach the BNPP site, using conservative assumptions about the magnitudes of volcanic eruptions and simplified numerical models of potential hazards. The remainder of this Chapter describes numerical and probabilistic techniques to estimate screening distance values for these phenomena. These values, in turn, are used to determine the capability of Mt. Natib, Mt. Mariveles, and Mt. Pinatubo volcanoes to affect the BNPP site.

9.3 Estimating screening distance values

Geological maps of the Mt. Natib volcanic deposits indicate that pyroclastic density currents and secondary lahar (volcanic mudflow) deposits occur in the BNPP site area (EBASCO, 1977; Newhall, 1979). The presence of these deposits is clear evidence that the BNPP site is located within a screening distance for these phenomena. A screening distance is defined as the distance from a volcano that a specific volcanic phenomena, such as pyroclastic flows, may plausibly reach (Hill *et al.*, Chapter 25, this volume). Screening distance depends on a number of factors, such as topography of the volcano, possible magnitudes of future eruptions and the types of volcanic phenomena involved. There is uncertainty in the estimate of screening distances, but, it is often practical to determine if a specific site is beyond, or within, a screening distance for specific phenomena originating from a volcano using scoping calculations. Such scoping calculations are used here to assess volcanic hazards at the Bataan site.

The site may be exposed to both proximal and distal effects of volcanic eruptions from Mt. Natib (Connor *et al.*, Chapter 3, this volume). In addition, the site may be exposed to far-field effects from Mt. Pinatubo and Mt. Mariveles volcanoes, particularly from tephra fallout. We can refine our understanding of potential hazards using a variety of numerical methods to consider the magnitudes of potential volcanic eruptions that produce phenomena that could impact the site. Analysis is limited to products of explosive eruptions, including tephra fallout, pyroclastic flows, and lahars. Other phenomena, such as new vent formation and lava flows are not considered in this chapter, and require additional analyses in order to assess their potential hazards to the BNPP site.

9.3.1 Hazards from tephra fallout

Tephra fallout creates loads on engineered structures and may disrupt ventilation, electrical and cooling systems at nuclear power plants. Thick tephra accumulation might render a site temporarily inoperable, and very rapid erosion of tephra deposits may generate potentially damaging lahars. The TEPHRA2 computer program (Bonadonna *et al.*, 2005; Bonadonna, 2006; Connor and Connor, 2006; Connor *et al.*, 2008) is used to estimate potential accumulations of tephra fallout at the BNPP site and on the flanks of Mt. Natib volcano above the BNPP site with a series of deterministic and probabilistic analyses. The numerical simulation of tephra accumulation is based on the advection-diffusion equation (Suzuki, 1983; Armienti *et al.*, 1988; Connor *et al.*, 2001), which is expressed by a simplified mass-conservation equation:

$$\frac{\partial C_j}{\partial t} + w_x \frac{\partial C_j}{\partial x} + w_y \frac{\partial C_j}{\partial y} - v_{l,j} \frac{\partial C_j}{\partial z} = K \frac{\partial^2 C_j}{\partial x^2} + K \frac{\partial^2 C_j}{\partial y^2} + \Phi \qquad (9.1)$$

where, x, y, and z are spatial coordinates expressed in meters; C_j is the mass concentration of particles (kg m^{-3}) of a given particle size class, j; w_x and w_y are the x and y components of the wind velocity (m s^{-1}); K is a horizontal diffusion coefficient for tephra in the atmosphere (m^2 s^{-1}); $v_{l,j}$ is the terminal settling velocity (m s^{-1}) for particles of size class, j, as these particles fall through a level in the atmosphere, l; Φ is the change in particle concentration at the source with time, t (kg m^{-3} s^{-1}). The algorithm implemented in TEPHRA2 assumes negligible vertical wind velocity and diffusion, and assumes a constant and isotropic horizontal diffusion coefficient ($K = K_x = K_y$). The terminal settling velocity, v, is calculated for each particle size, j, at each atmospheric level, l, as a function of the particle's Reynolds number, which varies with atmospheric density. Wind velocity is allowed to vary as a function of height in the atmosphere, but it is assumed to be constant within a specific atmospheric level.

Tephra fallout hazard studies are most concerned with mass accumulation at specific locations. TEPHRA2 calculates tephra accumulation, M (kg m^{-2}), at each location, (x, y):

$$M(x,y) = \sum_{l=0}^{H_{max}} \sum_{j=d_{min}}^{d_{max}} m_{l,j}(x,y) \qquad (9.2)$$

where, $m_{l,j}(x,y)$ is the mass fraction of the particle size, j, released from atmospheric level, l, accumulated at location, (x,y). H_{max} is the maximum height of the erupting column, and d_{min} and d_{max} are, respectively, the minimum and maximum particle diameters. Thus, the distribution of tephra mass following an eruption depends on both the distribution of mass in the eruption column and the distribution of mass by grain-size. The algorithm implemented in TEPHRA2 assumes that mass is uniformly distributed in the eruption column, or can be specified to be uniformly distributed in some fraction of the uppermost column, to be consistent with observations of strong volcanic plumes. Grain-size distribution is assumed to be log-normal, and is deduced from comparison with studies of well-preserved deposits.

Deterministic analysis Hazard assessments rely on probabilistic methods to accurately forecast the potential occurrence of disruptive phenomena. As part of this modeling process, deterministic assessments can be useful for estimating potential tephra accumulation resulting from eruptions of a specific size during specific meteorological conditions. For example, one can estimate tephra fallout at the BNPP resulting from a large-volume, explosive eruption of Mt. Natib, when the wind is blowing from the volcano toward the site. These analyses are accomplished by completely specifying the eruption and meteorological parameters, and calculating an isomass map based on these parameters using TEPHRA2. Such bounding calculations are particularly useful for estimating screening distances and may provide useful supplementary material for the interpretation of probabilistic assessments.

Five deterministic scenarios are presented based on the following eruption parameters: location of the vent, column height, total erupted mass and grain-size distribution. Meteorological parameters include wind direction and speed, as a function of elevation in the atmosphere. Eruptions span VEI 3−7 with associated maximum column heights (H_{max}) of 8, 14, 25, 35 and 45 km, respectively (Newhall and Self, 1982). A small VEI 3 eruption is represented by an 8 km-high erupting column. A 14 km-high column represents the approximate boundary between VEI 3 and VEI 4 eruptions; this column height is also the lower limit of sub-Plinian eruptions according to Pyle (1989). As EBASCO (1977, 1979) proposed an analysis of tephra hazard at the BNPP site based on analogy with the 1912 Katmai eruption, 25 km was selected to match the maximum column height of that VEI 5 eruption (Fierstein *et al.*, 1997). The 35 km column height reflects the 1991 eruption (VEI 6) of Mt. Pinatubo, and 45 km represents an upper limit scenario based on the historical eruption (VEI 7) of Tambora in 1815 (Sigurdsson and Carey, 1989).

Eruption duration, T, and maximum column height, H_{max}, are used to calculate the total erupted mass for each scenario, assuming steady-state conditions. Koyaguchi and Tokuno (1993) proposed an eruption duration of 5 hr for the 1991 climactic eruption of Mt. Pinatubo, based on the expansion of the umbrella cloud in the stratosphere. This is, perhaps, an over-estimate of eruption duration, as the umbrella cloud may have continued to expand in the stratosphere after cessation of appreciable mass discharge from the vent. Tahira *et al.* (1996) proposed an eruption duration of 3.5 hr, based on infrasonic and acoustic waves generated by the explosive eruption. According to Paladio-Melosantos *et al.* (1996), the peak

Table 9.1. *Eruption column height and total mass inputs for deterministic tephra models are based on analog eruptions and Volcano Explosivity Index (VEI).*

Parameter	**VEI 3**	**VEI 4**	**VEI 5**	**VEI 6**	**VEI 7**
Column height (km)	8	12	25	35	45
Total Mass (kg)	5.7×10^{9}	5.3×10^{10}	5.4×10^{11}	2.1×10^{12}	5.7×10^{12}

activity of the eruption was sustained for about 3 hr, followed by waning activity for 6 hr. For these deterministic scenarios, we chose an eruption duration of 3 hr, which maximizes flow rate for specific column heights.

For steady eruptions, the mass discharge rate of an eruption is empirically related to the column height (Sparks *et al.*, 1997):

$$H_{max} = 1.67Q^{0.259} \tag{9.3}$$

where, Q is the magma discharge rate ($\mathrm{m^3\,s^{-1}}$). From the density of the deposit (ρ_{dep}) and the duration of the eruption (T), the magma discharge rate (Q) is:

$$Q = \frac{M_o}{T\rho_{dep}} \tag{9.4}$$

where, M_o is the total mass of the deposit in kilograms. The bulk density of the deposit, ρ_{dep} ($\mathrm{kg\,m^{-3}}$), is assumed to be $1000\,\mathrm{kg\,m^{-3}}$, corresponding well with the average density of the 1991 phenocryst-rich dacitic pumice of Mt. Pinatubo ($977\,\mathrm{kg\,m^{-3}}$ proposed by Pallister *et al.*, 1996). This value is also in good agreement with the range $500-1500\,\mathrm{kg\,m^{-3}}$, the bulk density of known Plinian deposits (Sparks *et al.*, 1997). Total mass is related to eruption column height and eruption duration by:

$$M_o = T\rho_{dep}\left(\frac{H_{max}}{1.67}\right)^4 \tag{9.5}$$

Thus, assuming maximum eruption column heights, total eruption duration, and deposit density, total eruption mass is calculated for each scenario. Table 9.1 lists the the column heights and mass used by each scenario to estimate tephra accumulation at the BNPP site. For comparison, the VEI 6 scenario essentially matches source parameters that are described in the literature for the 1991 climactic Plinian eruption of Mt. Pinatubo (Koyaguchi and Tokuno, 1993; Holasek *et al.*, 1996; Koyaguchi, 1996; Paladio-Melosantos *et al.*, 1996; Rosi *et al.*, 2001).

Tephra dispersion also depends on the size distribution of particles (grain-size distribution) erupted from the volcano. Particle (clast) size distributions can be characterized in terms of several parameters (Inman, 1952): minimum and maximum volcanic clast diameter; median clast diameter (Md_ϕ); graphic standard de-

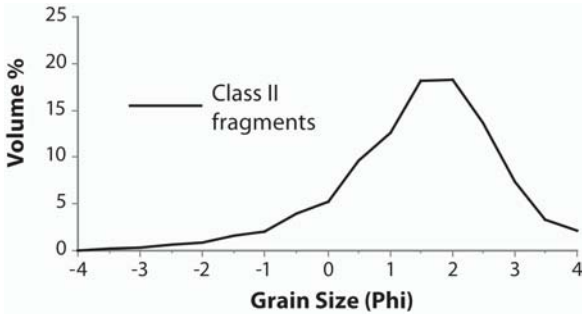

Fig. 9.2. The total grain-size distribution used in the tephra models is derived from analysis of the climactic Plinian eruption of Mt. Pinatubo in June 1991 (Class II fragments). Modified from Koyaguchi and Ohno (2001).

viation, or sorting (σ_ϕ); and the graphical skewness, a measure of the asymmetry of the grain-size distribution. Complete and reliable total grain-size distribution data for explosive volcanic eruptions are difficult to establish from field data and are rarely reported (Bonadonna and Houghton, 2005). Problems in determining the total grain-size distribution for an eruption stem from difficulty in sampling all facies of the deposit. Much of the tephra of the 1991 eruption of Mt. Pinatubo fell into the South China Sea (Wiesner *et al.*, 1995), so direct estimation of the total grain-size distribution is not practical. Nevertheless, based on a numerical model, Koyaguchi and Ohno (2001) proposed a grain-size distribution of class II fragments (pyroclasts that accumulate at medial distances from the vent) at the top of the eruption column for two depositional layers of the 1991 Plinian eruption of Mt. Pinatubo. Although not optimal, as proximal and distal pyroclasts are missing in Koyaguchi and Ohno's (2001) model, the grain-size data from those two tephra layers can be combined (Figure 9.2) to obtain a total grain-size distribution for the tephra fallout of the 1991 Plinian eruption. The median diameter of volcanic clasts is $1.35\,\phi$ ($\phi = -\log_2(d)$), d being the particle diameter in millimeters. The sorting of the deposit is $\sigma_\phi = 1.16\phi$, representing good sorting for tephra deposits (Fisher and Schmincke, 1984; Cas and Wright, 1987). These values are used for all simulations in the deterministic analysis of tephra fallout, although the actual total grain-size distribution of the 1991 eruption of Mt. Pinatubo may be finer and less sorted. The graphical skewness of the total grain-size distribution is assumed to be zero.

Tephra accumulation at a site is strongly dependent on wind speed and direction during the timespan of eruption. Two different wind estimates are used for each scenario. One estimate uses wind velocities averaged for the year 2006 based on reanalysis data from the National Center for Environmental Prediction Reanalysis

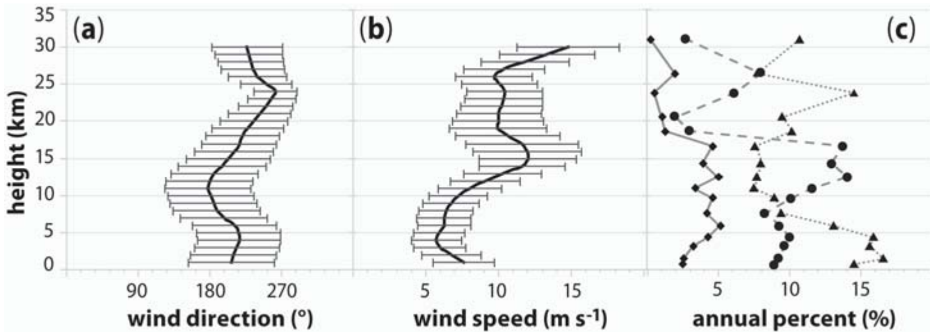

Fig. 9.3. Hazards associated with tephra fallout are strongly dependent on meteorological conditions. Here, a compilation of reanalysis data for the BNPP site illustrates the average (dark line) and one standard deviation (horizontal bars) of wind conditions in 2006, for (a) the direction toward which the wind is blowing and (b) wind speed (m s^{-1}), as a function of height above sea level. These data are used as input parameters for TEPHRA2 to estimate tephra accumulation in the site region. (c) Tephra deposition at the BNPP site is maximum when the wind blows from the volcano toward the site. The percentage of the time the wind blew toward the site (±15°) from Mt. Natib (circles), Mt. Pinatubo (diamonds) and Mt. Mariveles (triangles) is graphed as a function of height above sea-level.

project (Kalnay *et al.*, 1996). The reanalysis data consists of wind velocity estimates at 17 pressure levels which are are linearly interpolated to 30 heights from 1−30 km (above 30 km, wind conditions are assumed to be constant) at 1 km intervals (Figures 9.3a and b). The second estimate represents an upper limit, whereby the wind is assumed to blow toward the BNPP with a speed, at each level, similar to the average wind speeds from the reanalysis data for 2006. Wind conditions, very similar to this upper limit estimate, occurred in 2006 ~ 3% of the time for Mt. Pinatubo, ~ 9% of the time for Mt. Natib and ~ 11% of the time for Mt. Mariveles (Figure 9.3c).

Results of the different deterministic scenarios are given in Table 9.2. Estimated potential accumulation at the BNPP site varies from trace amounts to 3.6 m for a VEI 7 eruption at Mt. Natib with wind blowing toward the site. These thicknesses correspond to a range in dry tephra load of about 0.01 kg m^{-2} to 3600 kg m^{-2}. Rainfall saturates tephra deposits and may double these estimated loads (Blong 1984).

Isomass map are shown in Figure 9.4a−c. Note that the scenario presented in Figure 9.5a for Mt. Pinatubo shows many similarities with the isopach maps proposed for the 1991 eruption in the literature (Koyaguchi, 1996; Paladio-Melosantos *et al.*, 1996), although the latter are more circular and dispersed toward the WSW (Koyaguchi and Tokuno, 1993; Wiesner *et al.*, 1995; Koyaguchi, 1996; Paladio-Melosantos *et al.*, 1996). This discrepancy is due to wind direction. Average wind directions at stratospheric altitudes for 2006 were mainly toward the SW. Strato-

Table 9.2. *Tephra fallout thickness (cm) at the BNPP site for each eruption scenario in the deterministic analysis.*

Volcano	Wind field	VEI 3	VEI 4	VEI 5	VEI 6	VEI 7
Natib	wind 2006[1]	1.0	6.7	39	100	180
	max wind[2]	1.6	12	74	190	360
Mariveles	wind 2006	0.001	0.01	0.03	0.1	0.7
	max wind	0.4	5.3	36	98	200
Pinatubo	wind 2006	0.005	0.3	4.7	13	30
	max wind	0.01	0.5	8.0	26	58

[1]average wind velocity in 2006
[2]average wind speed in 2006, but wind blows toward site

spheric winds were more toward the west during the actual eruption. The model predicts a tephra fallout thickness at the site of ≈ 13 cm, roughly double the observed accumulation during the eruption of Mt. Pinatubo, owing to the difference in wind direction. Furthermore, although the effect of the passage of typhoon Yunya during the eruption had little effect on the settling of high-Reynolds-number particles (Rosi *et al.*, 2001), typhoon Yunya may have been responsible for more spherical dispersion of low- to intermediate-Reynolds-number clasts, resulting in the more spherical isopach maps proposed in the literature (Koyaguchi, 1996; Paladio-Melosantos *et al.*, 1996). Comparison of the eruption and the simulations suggest that had the wind blown toward the site on June 15^{th}, 1991, the BNPP might have experienced tephra fallout as thick as ~ 25 cm (Table 9.2).

Although average wind conditions for 2006 closely mimic the shape of the tephra deposit of the 1991 eruption of Mt. Pinatubo (Figure 9.4a), these conditions poorly estimate extreme events. As an example, a VEI 6 from Mt. Mariveles will deposit only 1 mm of tephra with the average wind conditions, while with the wind blowing toward the site, the tephra thickness could reach 1 m (Table 9.2). Figure 9.3c shows that this scenario (wind blowing toward the site) occurs $\sim 11\%$ of the time for Mt. Mariveles. The average wind conditions happen to deposit tephra away from the BNPP, but a large fraction of individual wind fields actually blows closer to the BNPP area.

These isomass maps also point to the possibility that secondary phenomena resulting from tephra fallout could potentially affect the site area. Although tephra accumulations at the BNPP site are not significant (e.g. not exceeding 10 cm) for many scenarios (e.g. $<$ VEI 6), lower explosivity eruptions on Mt. Natib may result in significant tephra accumulations up-slope from the site. Such deposits may be sufficient to remobilize and form lahars that could possibly affect the site area.

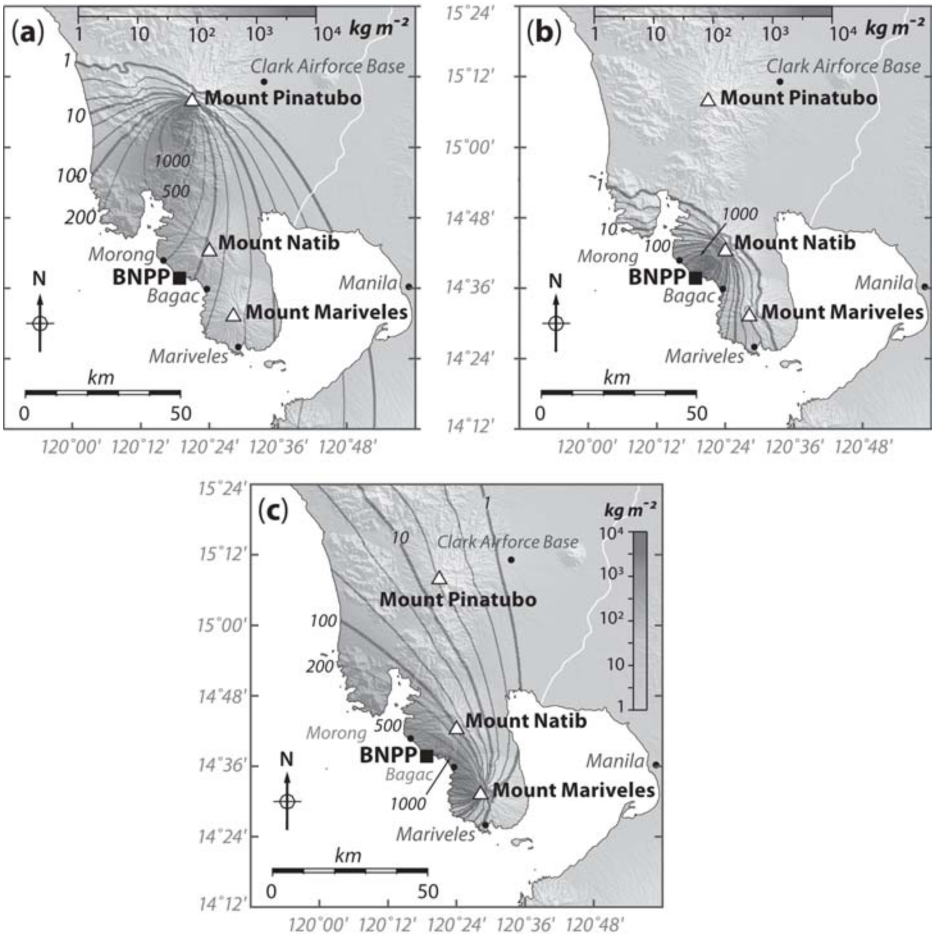

Fig. 9.4. Explosive eruptions of (a) Mt. Pinatubo, (b) Mt. Natib, and (c) Mt. Mariveles volcanoes may result in substantial accumulation of tephra at the BNPP site. These examples, based on output from TEPHRA2, show isomass maps for eruptions of various magnitudes and wind conditions. In (a) a VEI 6 eruption of Mt. Pinatubo during average wind conditions for 2006 results in an isomass map that is very similar to the actual tephra distribution following the 1991 eruption of Mt. Pinatubo. In this example, tephra accumulation at the site is ~ 100 kg m^{-2}, a mass load sufficient to cause damage to some structures, and to adversely affect electrical and water filtration systems. In contrast, a much smaller magnitude eruption, VEI 4, from Mt. Natib would potentially result in much larger tephra accumulation at the site, >1000 kg m^{-2} (b). In this simulation wind is assumed to blow from Mt. Natib toward the site at average speed as a function of elevation for the region. Similarly, the model suggests that a VEI 5 eruption of Mt. Mariveles would result in >1000 kg m^{-2} tephra accumulation at the site, if winds blew from the volcano toward the site. Contours are in mass of tephra accumulation per unit area (kg m^{-2}, dry, where (kg m^{-2} is roughly equivalent to 10 cm tephra thickness).

Probabilistic analysis Probabilistic methods more thoroughly assess the effects of random variation in eruption parameters and meteorological conditions on estimates of tephra accumulation. Our probabilistic analysis uses TEPHRA2 to calculate the distribution of tephra accumulation at the BNPP site for potentially explosive eruptions of Mt. Natib, Mt. Mariveles, and Mt. Pinatubo volcanoes. For each of the three source volcanoes, a Monte Carlo analysis is completed, each consisting of 1000 simulations. Eruption column height is randomly sampled from a log-uniform distribution of range 14−40 km. A log-uniform distribution is used because this truncates possible values at the lower limit of credible column heights for small explosive eruptions. As noted previously, this minimum column height (14 km) represents the approximate boundary between VEI 3−4. The upper bound of the range also has practical significance. Although higher columns may be possible, the properties of the atmosphere at these altitudes are such that higher columns would have little additional impact on the dispersion of tephra particles. The use of a logarithmic function reflects the higher frequency of lower-altitude volcanic plumes (Simkin and Siebert, 1994).

The total erupted mass of tephra is calculated using (9.5) from eruption duration and column height. Duration is randomly sampled from a uniform distribution of range 1−9 hr. This range is consistent with eruption durations reported for VEI 4−6 eruptions, and is consistent with the eruption duration for the 1991 Plinian eruption of Mt. Pinatubo (Koyaguchi and Tokuno, 1993; Tahira *et al.*, 1996; Paladio-Melosantos *et al.*, 1996). No correlation is assumed between eruption column height and eruption duration for the purpose of estimating total eruption mass. The resulting distribution of total eruption mass is log-normally distributed (Figure 9.5), emphasizing the higher probability of smaller eruptions (Simkin and Siebert, 1994).

Large variation in grain-size distribution appear possible for different types of Plinian eruptions from similar volcanoes. The 1991 Plinian eruption of Mt. Pinatubo has estimates of $Md_\phi = 1.35$, and $\sigma_\phi = 1.16$, for class II fragments at the top of the volcanic eruption column (Koyaguchi and Ohno, 2001). Typically, Md_ϕ estimates for entire tephra-fallout deposits might range from $-1.0\,\phi - 4.0\,\phi$, or even smaller (i.e. $Md_\phi = 4.4 - 4.8$ for the 1980 eruption of Mount St. Helens; Carey and Sigurdsson, 1982; Durant *et al.*, submitted). The variation in the sorting of a tephra fall deposit (σ_ϕ) may be smaller, $2\,\phi - 3\,\phi$ for Plinian eruptions. Given this uncertainty, Md_ϕ and σ_ϕ are sampled from uniform distributions with ranges of $-1\,\phi$ to $5\,\phi$, and $2\,\phi$ to $3\,\phi$, respectively. No correlation is assumed between these grain-size distribution parameters and column height or eruption mass.

Reanalysis data are, again, used to describe the variation in wind velocity with height; a set of 1460 wind profiles (acquired 4 times daily during 2006, Kalnay *et*

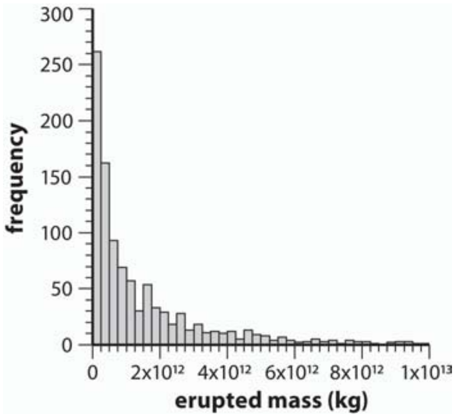

Fig. 9.5. Log-normally distributed values for total amount of tephra erupted (kg). The probabilistic assessment of tephra fallout randomly chooses total eruption mass values from this log-normal distribution. The range of possible values is initially calculated from a range of probable eruption column heights and eruption durations.

al., 1996) are randomly sampled. Although the eruption duration may be longer than 6 hr, only one randomly selected profile per simulation is used.

Results of this probabilistic analysis indicate that tephra accumulation at the BNPP site from possible eruptions of Mt. Natib and Mt. Mariveles would likely exceed tephra accumulation from possible eruptions of Mt. Pinatubo, by approximately one order of magnitude (Figure 9.6a). For comparison, the EBASCO (1979) hazard curve (Figure 9.6b) indicates that the probability of exceeding 1 m tephra accumulation at the site, given an explosive eruption of Mt. Natib, is $\approx P\{\text{accumulation} > 1\text{ m} \mid \text{explosive eruption}\} = 55\%$. However, using TEPHRA2, all calculated hazard curves, given an explosive eruption of Mt. Natib, yield lower probabilities for exceeding 1 m of tephra accumulation at the BNPP site. It appears that the EBASCO (1979) assessment using Mt. Katmai analog eruption data, may overestimate the tephra-fall hazard at the site compared to the results of numerical simulation.

The results of probabilistic analyses can also be represented as probability maps. These maps show the probability of exceeding a given threshold of tephra accumulation over an area of interest. Thresholds of tephra accumulation can be chosen to reflect potential damage to buildings (i.e. tephra load leading to partial or complete roof collapse) in the area, potential accumulation that might lead to lahar formation, or reflect design factors for NPP structures. A value of 10 cm reflects the onset of roof collapse, 20 cm reflects widespread roof collapse, especially if the tephra layer is saturated with water (Spence *et al.*, 1996). The probability of tephra accumulation exceeding 100 kg m^{-2} (dry accumulation, $\approx$ 10 cm in thickness) in the

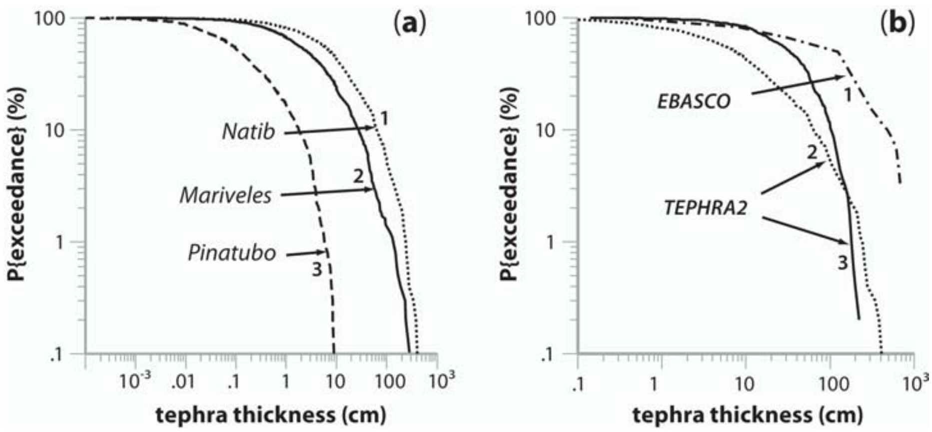

Fig. 9.6. Hazard curves show the conditional probability of exceeding different thicknesses of tephra at the location of the BNPP, given a volcanic eruption. Graph (a) compares tephra thicknesses modeled for Natib (1), Mariveles (2), and Pinatubo (3). The curves were generated from TEPHRA2 output, based on 1000 simulations using wind values randomly selected from reanalysis data for 2006 and eruption parameters randomly selected from a range of explosive eruption conditions. This graph indicates that given an eruption, tephra accumulation at the BNPP from eruptions of Mt. Natib and Mt. Mariveles are similar, and would likely exceed tephra accumulations associated with a Mt. Pinatubo eruption by one order of magnitude. Graph (b) compares the EBASCO hazard curve, based on the 1912 eruption of Mt. Katmai in Alaska (1), with two hazard curves generated by 1000 simulations using TEPHRA2: curve 2 is identical to curve 1 in graph (a), curve 3 is based on eruption parameters similar to the 1991 eruption of Mt. Pinatubo and a random wind field, also based on 2006 reanalysis data. This graph indicates that using the 1912 Katmai eruption as an analog for tephra accumulation overestimates the hazard at the site by approximately one order of magnitude. These curves could be weighted by the probability of occurrence as part of a comprehensive hazard assessment.

region around the BNPP is shown in Figure 9.7 and is $\approx 55\%$ near the BNPP site. Of course, roofs of nuclear facilities may be designed to withstand higher loads than typical buildings and houses. Nevertheless, the probability map indicates that widespread damage to community infrastructure in the region of the NPP is likely in the event of an eruption of significant intensity (e.g. $\geq$ VEI 4). Such conditions are important to consider in site suitability assessment and design (Hill *et al.*, Chapter 25, this volume).

The probability map also indicates that the central part of Mt. Natib, and the W and SW flanks of the volcano are the most likely areas to be subjected to tephra fallout. This indicates that in the event of an explosive eruption, lahars would likely occur, potentially over widespread areas, on this flank of the volcano. These lahars would impact community infrastructure and possibly directly impact the BNPP site area.

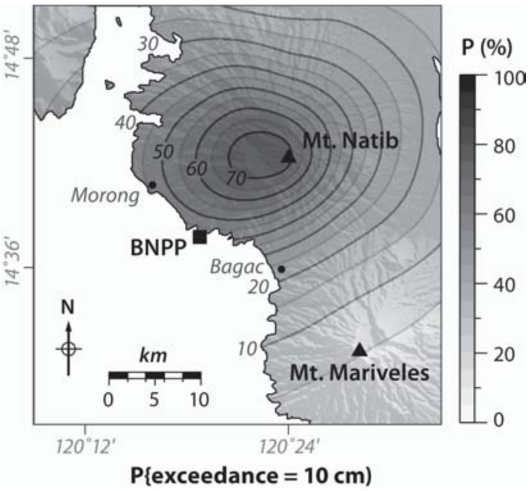

Fig. 9.7. Map contours the probability of tephra accumulation exceeding 10 cm ($\sim$100 kg m^{-2}), given an explosive eruption of Mt. Natib. Note that these simulations indicate that tephra accumulation is most likely on the W and SW flanks of Mt. Natib, suggesting these areas are potential sources for lahars following explosive volcanic activity. Map contoured in 5% intervals.

In summary, it appears that the BNPP site is located within the screening distance for tephra fallout from both Mt. Natib and Mt. Mariveles. A screening threshold of approximately 10 cm tephra accumulation is used, based on a damage threshold commonly observed for residential and commercial buildings. A different screening threshold may be desirable for nuclear facilities, which may have greater resiliency for roof loads, but may be more sensitive to particulates in water and electrical systems. In a comprehensive hazard analysis, the design of the facility should be evaluated for the range of tephra loads such as those described in our analysis (cf. Hill *et al.*, Chapter 25, this volume).

9.3.2 Lahar source regions

Several types of volcanic phenomena, such as pyroclastic flows and lahars, can be strongly influenced by topography. Estimation of screening distance values for these volcanic phenomena should account for major topographic features of the volcano and of the site. On Mt. Natib volcano, for instance, a steep caldera wall on the west side of the volcano may prevent many types of flows that originate in the caldera from reaching the site. Instead, such flows might drain from the caldera through a break in its NW rim (EBASCO, 1977). It is therefore somewhat counter-intuitive that pyroclastic flow deposits and lahars are mapped at the BNPP site. Either these units were deposited when the volcano had a much different form, prior to the formation of the summit caldera, or these phenomena can reach the site area despite the topographic barrier provided by the western caldera rim. The purpose of screening distance value calculations is to determine whether such flows could reasonably develop in the future, considering current or likely future conditions.

On Mt. Pinatubo volcano, lahars were generated as a result of the accumulation of pyroclastic material (e.g. tephra and pyroclastic flow deposits) on steep slopes and as a result of tropical rainfalls that worked to erode these deposits rapidly (Daag, 2003). For potential lahars from Mt. Natib, experience on Mt. Pinatubo volcano (Newhall and Punongbayan, 1996) suggests that complex scenarios accompany explosive volcanic eruptions, and these scenarios might cause lahar source regions to develop outside the caldera, including high on the west flank of the volcano. The exceedance probability map for tephra accumulation in the site region makes it clear that if explosive activity were to occur on Mt. Natib or a nearby volcano, conditions for lahar formation may develop (Figure 9.7). The steep slopes on the west and south flanks of Mt. Natib could serve as source regions for lahars that would descend river valleys lower on flanks of the volcano.

Several different models can be used to assess the potential hazard posed by lahars to the BNPP site. For example, a statistical model, such as LAHARZ (Iverson *et al.*, 1998) might be used to assess potential flow-paths. Daag (2003) proposed a water runoff model for lahars following the 1991 eruption of Mt. Pinatubo to predict lahar runout and magnitude, utilizing a cell-based distributed model coupled with a high resolution digital elevation model (DEM). Daag's (2003) model is catchment-scale and uses physical laws of flow dynamics to describe lahars on Mt. Pinatubo. Although these models help delineate potential areas of lahar inundation, they require high resolution (i.e. ideally < 10 m grid) digital elevation data that are currently not available for the Mt. Natib region. Here, we focus on the coupled nature of tephra fallout and lahar generation by considering two empirical models. The first model is based on the potential for gravitationally induced failure of the tephra deposit on the volcano slopes (Iverson, 2000), thus triggering lahars. The second model is based on the increase in water and sediment runoff as tephra accumulates (Daag, 2003; Yamakoshi *et al.*, 2005).

Iverson's (2000) model assumes that slope failure is described by a Coulomb failure criterion expressed as a yield condition:

$$|\tau| = c + \sigma_n \tan\beta \tag{9.6}$$

where τ is shear stress, c is tephra cohesion, σ_n is normal stress (perpendicular to the slope) and β is the angle of internal friction. This Coulomb failure model can be expressed as a ratio of resistive and driving forces, known as the Factor of Safety

(FS):

$$FS = \frac{ResistingForce}{DrivingForce} = \frac{c + \sigma_n \tan\beta}{|\tau|} \tag{9.7}$$

where $\tau = -Zy_t \sin\alpha$, $\sigma_n = Zy_t \cos\alpha$, Z is the layer thickness (here derived from estimates of potential tephra accumulation), y_t is the total unit weight of the deposit per unit area and α is the slope of the slip surface (pre-tephra deposition topography). It follows that:

$$FS = \frac{c}{Zy_t \sin\alpha} + \left(1 - \frac{y_w}{y_t}\right)\frac{\tan\beta}{\tan\alpha} \tag{9.8}$$

where y_w is the unit weight of water added to the deposit by rainfall. Slope failure occurs when $FS < 1$. Lahars will be generated primarily on steep slopes after deposition of tephra units that become saturated by water infiltration, greatly reducing the shear strength of these tephra layers (Daag, 2003). This slope failure model for lahar generation is thus coupled to a tephra fallout model, and, assuming deposit saturation by infiltrating water, areas of likely slope failure ($FS < 1$) can be inferred (Figure 9.8a).

The actual slope failure process depends on the nature of the slope geology (i.e. infiltration, strength characteristics) underlying the potential tephra deposit and the cover of vegetation, grain-size properties of the tephra fallout and infiltration rates both into the tephra deposit and into the underlying units. These factors are complex, spatially variable and not explicitly addressed by the Iverson (2000) model, but should be considered in interpreting model results. Given these caveats, a Factor of Safety map (Figure 9.8a) indicates zones of potential lahar generation, from where those flows may follow main drainages and inundate areas lower on the flanks of the volcano, an idea completely consistent with the screening distance calculation.

The potential lahar source region (Figure 9.8a) covers an area of about 12 km^2. The corresponding total volume of tephra deposit occurring on these steep slopes ($FS < 1$) is 1.7×10^7 m^3. Iverson *et al.* (1998) developed an empirical relationship between lahar volume and the planimetric area inundated by lahars, based on their analysis of numerous lahar deposits: $B = 200V^{2/3}$, where B (m^2) is the area inundated by a lahar of volume V (m^3). Using this relationship, the planimetric area inundated by one or more lahars resulting from slope failure is about 13 km^2, a moderate lahar event, comparable to the one that occurred at Nevado del Ruiz volcano in 1985 (see Connor *et al.*, Chapter 3, this volume). Therefore, this model suggests that areas on the southwest flank of the volcano would potentially be impacted by lahars following explosive volcanic activity.

Alternatively, lahars can be triggered when even thin, fine-grained tephra layers accumulate, because these layers may impede infiltration and increase surface

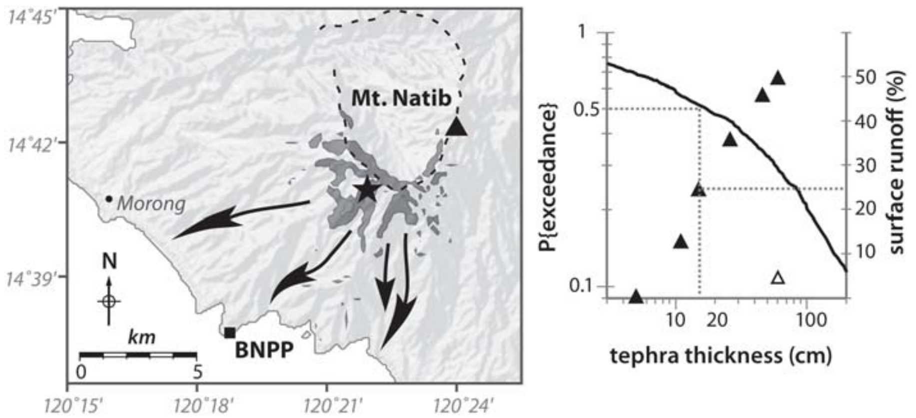

Fig. 9.8. (a) Potential lahar source regions (dark shaded areas) resulting from a hypothetical VEI 5 eruption from Mt. Natib (wind blowing toward the site), identified as those areas where the Factor of Safety, $FS \leq 1$. Arrows highlight main drainages on the SSW part of Mt. Natib where lahars have the potential to occur and affect the NPP site region. Black star indicates the location for the hazard curve shown in (b). (b) Exceedance probability, based on the VEI 5 eruption used in (a), and surface runoff % (100× water and sediment runoff divided by the amount of rainfall) plotted as a function of tephra thickness. This plot indicates that lahar potential increases with higher tephra accumulation and higher runoff. Surface runoff vs. tephra thickness values (solid triangles) are for fine-grained tephra on Miyakejima volcano (Japan), modified after Yamakoshi *et al.* (2005). Runoff is diminished for coarse-grained deposits (open triangle) on Miakejima volcano. For example, given an explosive eruption (VEI 5) of Mt. Natib, the TEPHRA2 model indicates that the probability of tephra exceeding 17 cm is 50%. Empirical observations on Miyakejima volcano suggest that for this thickness of tephra, ~ 25% of rainfall and sediment by volume will runoff into drainages, forming hyper-concentrated flows.

runoff (Yamakoshi *et al.*, 2005). In a study of lahar generation following recent eruptions of Miyakejima volcano, Yamakoshi *et al.* (2005) found a positive, non-linear correlation between tephra thickness and decreased infiltration, resulting in increased surface runoff that may trigger lahars with very low sediment load by volume. Such flows are called hyperconcentrated flows. Essentially, as the tephra deposit gets thicker, water is less likely to infiltrate the whole tephra deposit, thus increasing potential surface runoff. Daag (2003) observed, from rainfall simulations on tephra deposits from Mt. Pinatubo, that tephra fallout deposits have low infiltration capacities due to the abundance of fine particles, thus increasing water runoff. In applying this alternative model, a hazard curve for tephra accumulation in a specific area up-slope of the site can be evaluated in terms of lahars triggered by increased run-off of surface water and tephra (Figure 9.8b).

The hazards due to hyperconcentrated flows are different that those associated with slope failure. Rather than a single voluminous debris flow, the increased surface runoff results in persistent hyperconcentrated flows and floods, which may continue to affect the area at the base of the volcano for years following the eruption. Individual events, however, are of much smaller volume. For example, in response to 9 mm rainfall and using the empirical relationship shown in Figure 9.8b, the tephra deposit would cause an increase in runoff of approximately 4×10^5 m^3. As with larger volume debris flows, these persistent hyperconcentrated flows would adversely affect the region on the southwest flank of the volcano.

It appears that tephra dispersal can potentially result in flow-paths for lahars toward the site vicinity, following the major drainages on Mt. Natib southern flanks (Figure 9.8a), despite near-vent topographic barriers presented by the caldera wall. Because tephra deposition would likely be widespread on the southwest flank of the volcano following an explosive eruption, the nature of sedimentation on this flank of the volcano would change, resulting in lahars, hyperconcentrated flows and/or water floods. This coupled nature of volcanic phenomena is quite important to consider in estimation of screening distance values.

Cumulatively, these analyses indicate that the BNPP site is within screening distance for lahars, given their potential volume and the areas potentially inundated by them. Of course, the geographic position of the BNPP site on Napot Point may protect the site from inundation by lahars. Comprehensive analysis of lahar flow-paths with a high-resolution DEM may verify this possibility. Regardless, lahars would significantly disrupt roads and communities in the site region, a factor important to determination in site suitability.

9.3.3 Hazards from pyroclastic density currents

Topographic barriers also may prevent future pyroclastic density currents from reaching the BNPP site. We consider a basic but widely used model (i.e. the energy cone model; Sheridan, 1979) for the potential runout of pyroclastic density currents for the purposes of evaluating this potential hazard, and to determine if the site lies within or beyond a screening distance value that is representative for such highly mobile flows. The energy cone model was first proposed by Sheridan (1979; also see Connor *et al.*, Chapter 3, this volume). Essentially this model uses the height, H, from which pyroclastic density currents originate, directly related to the potential energy of the flows, to estimate their runout, L, the horizontal distance the flows are likely to travel from their source. The ratio, H/L depends on the mobility of the pyroclastic density current. Examples in the literature commonly range from $H/L = 0.2$ for small flows, to $H/L < 0.01$ for large-volume, highly mobile pyroclastic density currents.

For pyroclastic density currents originating from dome-building eruptions (e.g. the ongoing eruption of Soufrière Hills volcano, Montserrat) and from low-volume

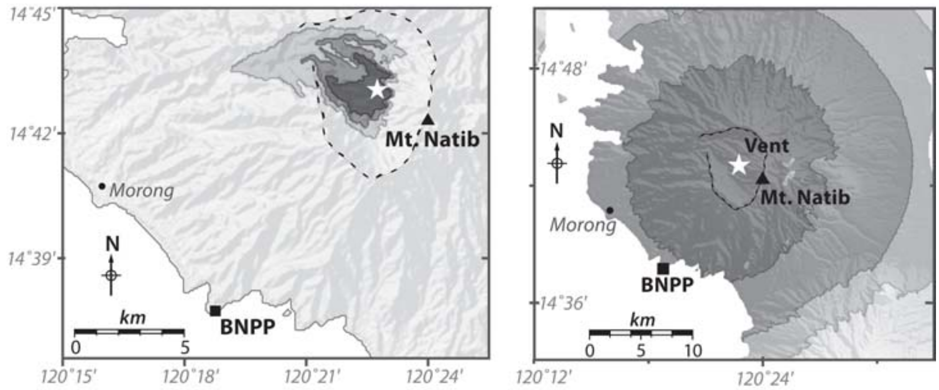

Fig. 9.9. (a) Three potential pyroclastic flow runouts from the caldera floor of Mt. Natib, estimated using the energy cone model. The 3 gray-shaded regions represent possible areas inundated by pyroclastic flows originating from the collapse of a 100 m-high dome. The different shaded regions represent areas inundated by pyroclastic flows of increasing potential energy, represented by the ratio of dome height to runout length: $H/L = 0.2$ (darkest gray area), $H/L = 0.15$ (medium gray area), $H/L = 0.1$ (light gray area). Uncertainty in the appropriate value of H/L results in uncertainty in the total runout of the flow. In all of these cases, the pyroclastic flows do not overtop the caldera wall, and thus flow away from the BNPP site. (b) In contrast, higher release heights (e.g., 1000 m above the caldera floor) associated with eruption column collapse and higher intensity eruptions result in inundation of the BNPP site. Shaded areas show inundation by pyroclastic density currents for $H/L = 0.15$ (closest to the vent, darkest shading), $H/L = 0.1$, and $H/L = 0.075$ (farthest from the vent, lightest shading).

explosive eruptions (< VEI 5), our analysis shows that the caldera wall will likely act as a topographic barrier for pyroclastic flows traveling toward the site from a central vent eruption of Mt. Natib. Such flows would have insufficient potential energy to overcome the 300–500 m-high topographic barrier of the caldera wall and likely would be channelized toward the northwest, possibly exiting the caldera through a gap in the caldera wall (Figure 9.9a). Therefore, assuming low-energy explosive eruptions occur within the existing caldera, the site seems to be outside the screening distance for pyroclastic density currents released from comparatively low-lying sources within the caldera.

In the case of an explosive eruption of ~ VEI 5 or greater, or an eruption occurring from a new vent located on the southern flanks of the volcano, the energy cone model suggests that pyroclastic density currents may reach the site. Flows associated with such eruptions often generate pyroclastic density currents as a result of collapse of the eruption column or by boiling-over of a particularly dense eruption column. In such circumstances, the potential energy of the flow may be sufficient to overcome topographic barriers approximately 500 m-high, such as the caldera wall. Based on the energy cone model, a potential column collapse assumed to initiate at the top of the gas-thrust region (Connor *et al.*, Chapter 3, this volume), would need to originate at no more than 1 km elevation above the caldera floor. Once overcoming the southwest wall of the caldera, the topographic slope is such that the flow extends beyond the site area for $H/L < 0.15$ (Figure 9.9b). Based on this simplified analysis, it appears that the BNPP site is located within the screening distance value of pyroclastic density currents for eruptions VEI 5 or greater. As is the case for tephra fallout, such flows could also generate voluminous lahars, which may have the potential to affect the site.

Numerical models of pyroclastic density currents (e.g. Todesco *et al.*, 2002) might greatly improve this assessment and could be considered as part of a comprehensive hazard analysis for pyroclastic density currents. The energy cone calculation strongly suggests such an assessment would be useful for understanding a range of pyroclastic density current hazards for the BNPP site. In addition, a complete analysis of hazards also should consider the potential for new vent formation on the flanks of Mt. Natib. As observed at other composite volcanoes, such vents might also be a source of pyroclastic density currents that may create additional hazards at the site.

Concluding remarks

This analysis is intended to illustrate several important steps in a volcanic hazard assessment for nuclear facilities. For the BNPP site, this means using available data and available numerical methods to assess the capability of nearby volcanoes to erupt in the future and to produce potentially hazardous phenomena at the site. Do Mt. Natib, Mt. Mariveles and Mt. Pinatubo have a credible potential for future eruptions? Future eruptions appear highly likely from Mt. Pinatubo, considering its last explosive eruption in 1991 and many other eruptions in the Holocene. Several lines of evidence indicate that future eruptions from Mt. Natib and Mt. Mariveles are credible, including the existence of an active hydrothermal system within Mt. Natib volcano, the presence of little-eroded volcanic features (e.g. caldera depressions truncating both Mt. Natib and Mt. Mariveles), and probabilistic assessment based on the estimated repose since the last dated eruptive event. The probability estimate is highly uncertain, due to uncertainties in ages of past eruptions and possibly underestimates recurrence rate due to poor preservation of smaller eruptions in the geologic record. This uncertainty supports a conservative approach to hazards assessment that assumes future eruptions are possible from Mt. Pinatubo, Mt. Natib and Mt. Mariveles.

We have made such a preliminary assessment for a subset of potential volcanic phenomena utilizing a screening distance value approach. This analysis, made using relatively simple and widely available numerical techniques, indicates that the

BNPP site has the potential to be affected by phenomena such as tephra fallout, lahars, and pyroclastic density currents in the event of a future eruption. Cumulatively, these analyses indicate that Mt. Natib and Mt. Mariveles and, for tephra-fall hazards, Mt. Pinatubo, are capable volcanoes, following the definition provided by Hill *et al.* (Chapter 25, this volume).

Identification of Mt. Natib and Mt. Mariveles as capable volcanoes indicates that a more comprehensive volcanic hazard assessment appears warranted for the BNPP site. Goals of such a comprehensive assessment would include analysis of the current state of volcanic unrest at both Mt. Natib and Mt. Mariveles through implementation of monitoring techniques, such as a seismic network on the volcano, deformation monitoring, and perhaps seismic tomography to ascertain the origin and extent of the hydrothermal system within the volcano. Similarly, geochemical analyses might be extremely useful to delineate a magmatic component in thermal springs located in the caldera of Mt. Natib. A second goal of the comprehensive assessment would be to map these two volcanoes in sufficient detail to develop a more complete understanding of each volcano's stratigraphy, and to place radiometric dates in stratigraphic context. An integrated program including new radiometric dates and paleomagnetic analysis appears critical to developing a suitable record of past volcanic activity. Such a geologic program would be necessary in order to more fully assess the probability of future volcanism, the timing of most recent volcanism, and the important characteristics of past eruptions. Finally, more detailed analysis of volcanic hazards could make full use of a variety of numerical models that might further elucidate site hazards, particularly of lahar and pyroclastic flow phenomena. All of these numerical models of surface flows require use of a high-resolution (preferably < 10 m resolution) digital elevation model, which was not available to the authors at the time of this analysis. Acquisition of such a model would be an important step in the volcanic hazard assessment. Regardless of the details involved, the analyses presented herein demonstrate that several capable volcanoes exist within the area of the BNPP site. Based on recommendations in, for example, Hill *et al.* (Chapter 25, this volume), a comprehensive analysis appears necessary to support discussions or decisions regarding the suitability of the BNPP site.

This case study also illustrates some general factors to consider in volcanic hazard assessments of nuclear facilities. The timing and recurrence rate of volcanism at Mt. Natib and Mt. Mariveles are a major source of uncertainty in estimates of the likelihood of future activity. It is unlikely that the probability of future eruptions from Mt. Natib and Mt. Mariveles could be narrowed much below one order of magnitude by additional analyses, unless the global stratigraphic and chronological framework of these volcanoes were improved or very young volcanic deposits were identified. This is a common situation where nuclear facilities are considered in volcanically active regions. Screening based on the probability of occurrence of volcanic eruptions may have large uncertainties, giving a weak basis for decision making.

Screening distances are an effective method of assessing the potential for various phenomena to impact a site. Numerical techniques can have an important role to play in estimating these screening distances. For example, EBASCO (1977) did not have methods to simulate tephra fallout at the BNPP site numerically. Instead, a large eruption from a presumably analogous volcano was used. This resulted in a possible overestimate of potential tephra fallout hazards at the site. In contrast, probabilistic models yield hazard curves for the BNPP site that reasonably reproduced observed deposits from the 1991 Mt. Pinatubo. The great advantage of these models is that various scenarios of activity can be evaluated, providing a more robust perspective on the parameters that contribute to the potential hazards at the site.

Similarly, at the time of siting of the BNPP, it was argued that the topography of the Mt. Natib summit caldera protects the site from potential pyroclastic flows. This effect appears supportable for relatively small eruptions ($<$ VEI 5), but our analysis suggests pyroclastic flows from $>$ VEI 5 eruptions may reach the site. Furthermore, the coupled nature of volcanic phenomena (e.g., the potential of lahars resulting from tephra fallout) warrants further consideration. Fortunately, volcanology now possesses many of the tools required to make such assessments at an appropriate level of detail.

Further reading

Articles in the volume *Statistics in Volcanology* (Mader *et al.*, 2006) provide an overview of the literature on the timing of volcanic eruptions and forecasting activity at long-dormant volcanoes. The TEPHRA2 code is freely available on the worldwide web (Connor *et al.*, 2008). Modeling of volcanic phenomena is evolving rapidly. Models of volcanic eruptions and eruption phenomena are widely discussed in the *Bulletin of Volcanology* and *Journal of Volcanology and Geothermal Research*. See *Fire and Mud* (Newhall and Punongbayan, 1996) for comprehensive discussion of the eruptions of Mt. Pinatubo.

This manuscript was improved by the comments of Neil Chapman, Britt Hill, and an anonymous reviewer. ACMV was supported by a grant from the University of South Florida.

References

Armienti, P., G. Macedonio and M. T. Pareschi (1988). A numerical-model for simulation of tephra transport and deposition: Applications to May 18, 1980, Mount-St-Helens eruption. *Journal of Geophysical Research*, **93**, 6463−6476.

Blong, R. J. (1984). *Volcanic Hazards: A Sourcebook on the Effects of Eruptions*. Sydney: Academic Press.

Bonadonna, C. (2006). Probabilistic modelling of tephra dispersion. In: Mader, H. M., S. G. Cole, C. B. Connor and L. J. Connor (eds) *Statistics in Volcanology*, Special Publications of IAVCEI **1**. London: Geological Society, 243−259.

Bonadonna, C., C. B. Connor, B. F. Houghton, *et al.* (2005). Probabilistic modeling of tephra dispersal: Hazard assessment of a multiphase rhyolitic eruption at Tarawera, New Zealand. *Journal of Geophysical Research*, **110**, doi:10.1029/2003JB002896.

Bonadonna, C. and B. F. Houghton (2005). Total grain-size distribution and volume of tephra-fall deposits. *Bulletin of Volcanology*, **67**, 441−456.

Cabato, M. E. J. A., K. S. Rodolfo and F. P. Siringan (2005). History of sedimentary infilling and faulting in Subic Bay, Philippines revealed in high-resolution seismic reflection profiles. *Journal of Asian Earth Sciences*, **25**, 849−858.

Carey, S. and H. Sigurdsson (1982). Influence of particle aggregation on deposition of distal tephra from the May 18, 1980, eruption of Mount St. Helens volcano. *Journal of Geophysical Research*, **87**, 7061−7072.

Cas, R. A. F. and J. V. Wright (1987). *Volcanic Successions, Modern and Ancient: A Geological Approach to Processes, Products, and Successions*. Berlin: Springer Verlag.

CGIAR-CSI (2004). Void-filled seamless SRTM data V1, International Centre for Tropical Agriculture (CIAT). CGIAR−Consortium for Spatial Information, SRTM 90 m Database, http://srtm.csi.cgiar.org

Connor, C. B., B. E. Hill, B. Winfrey, N. M. Franklin and P. C. La Femina (2001). Estimation of volcanic hazards from tephra fallout. *Natural Hazards Review*, **2**, 33−42.

Connor, C. B., A. R. McBirney and C. Furlan (2006). What is the probability of explosive eruption at a long-dormant volcano? *In*: Mader, H. M., S. G. Cole, C. B. Connor and L. J. Connor (eds) *Statistics in Volcanology*, Special Publications of IAVCEI **1**. London: Geological Society, 39−46.

Connor, L. J. and C. B. Connor (2006). Inversion is the key to dispersion: understanding eruption dynamics by inverting tephra fallout. *In*: Mader, H. M., S. G. Cole, C. B. Connor and L. J. Connor (eds) *Statistics in Volcanology*, Special Publications of IAVCEI **1**. London: Geological Society, 231−242.

Connor, L. J., C. B. Connor and C. Bonadonna (2008). Forecasting tephra dispersion using TEPHRA2. http://www.cas.usf.edu/c̃connor/vg@usf/tephra.html.

Daag, A. S. (2003). Modelling the erosion of pyroclastic flow deposits and the occurrences of lahars at Mt. Pinatubo, Philippines. Unpublished PhD thesis, ITC Dissertation number 104. Utrecht: University of Utrecht.

D'Amato, A. and K. Engel (1988). State responsibility for the exportation of nuclear power technology. *Virginia Law Review*, **74**, 1011−1066.

Defant, M. J., R. C. Maury, E. M. Ripley, M. D. Feigenson and D. Jacques (1991). An example of island-arc petrogenesis: geochemistry and petrology of the southern Luzon Arc, Philippines. *Journal of Petrology*, **32**, 455−500.

Durant, A. J., W. I. Rose, A. M. Sarna-Wojcicki, S. Carey and A. C. M. Volentik (in press). Hydrometeor-enhanced tephra sedimentation: constraints from the 18 May 1980 eruption of Mount St. Helens (USA). *Journal of Geophysical Research*, doi:10.1029/2008JB005756

EBASCO (1977). Preliminary safety analysis report, Philippine Nuclear Power Plant #1.

Philippine Atomic Energy Commission Open-File Report and response to questions. Manila: Philippine Atomic Energy Commission.

EBASCO (1979). Evidence substantiating the incredibility of volcanism on the west flank of Mt. Natib, and the assessment of volcanic hazards at Napot Point. Response to Philippine Atomic Energy Commission question #3. Manila: Philippine Atomic Energy Commission.

Efron, B. and R. Tibshirani (1991). Statistical data analysis in the computer age. *Science*, **253**, 390−395.

Fierstein, J., B. F. Houghton, C. J. N. Wilson and W. Hildreth (1997). Complexities of Plinian fall deposition at vent: an example from the 1912 Novarupta eruption (Alaksa). *Journal of Volcanology and Geothermal Research*, **76**, 215−227.

Fisher, R. V. and H.-U. Schmincke (1984). *Pyroclastic Rocks*. Berlin: Springer Verlag.

Holasek, R. E., S. Self and A. W. Woods (1996). Satellite observations and interpretation of the 1991 Mount Pinatubo eruption plumes. *Journal of Geophysical Research*, **101**, 27 635−27 655.

Inman, D. L. (1952). Measures for describing the size distribution of sediments. *Journal of Sedimentary Petrology*, **22**, 125−145.

IAEA (1978). Report of the IAEA Safety Mission to the Philippines Nuclear Power Plant No.1. Vienna: International Atomic Energy Agency.

Iverson, R. M. (2000). Landslide triggering by rain infiltration. *Water Resources Research*, **36**, 1897−1910.

Iverson, R. M., S. P. Schilling and J. W. Vallance (1998). Objective delineation of lahar-inundation hazard zones. *Geological Society of America Bulletin*, **110**, 972−984.

Kalnay, E., M. Kanamitsu, R. Kistler, *et al.* (1996). The NCEP/NCAR 40-year reanalysis project. *Bulletin of the American Meteorological Society*, **77**, 437−471.

Koyaguchi, T. (1996). Volume estimation of tephra-fall deposits from the June 15, 1991, eruption of Mount Pinatubo by theoretical and geological methods. *In*: Newhall, C. G. and R. S. Punongbayan (eds) *Fire and Mud*. Seattle: University of Washington and Quezon City: PHIVOLCS, 583−600.

Koyaguchi, T. and M. Ohno (2001). Reconstruction of eruption column dynamics on the basis of grain size of tephra fall deposits: 2. Application to the Pinatubo 1991 eruption. *Journal of Geophysical Research*, **106**, 6513−6534.

Koyaguchi, T. and M. Tokuno (1993). Origin of the giant eruption cloud of Pinatubo, June 15, 1991. *Journal of Volcanology and Geothermal Research*, **55**, 85−96.

Mader, H. M., S. G. Cole, C. B. Connor and L. J. Connor (eds) (2006). *Statistics in Volcanology*, Special Publications of IAVCEI **1**. London: Geological Society of London.

Newhall, C. G. (1979). Review of volcanologic discussions in the PSAR and related documents, Philippine Nuclear Power Plant #1. Washington D. C.: US Nuclear Regulatory Commission.

Newhall, C. G. and S. Self (1982). The Volcanic Explosivity Index (VEI): An estimate of explosive magnitude for historical volcanism. *Journal of Geophysical Research*, **87**, 1231−1238.

Newhall, C. G. and R. S. Punongbayan (1996). *Fire and Mud*. Seattle: University of Washington and Quezon City: PHIVOLCS.

Newhall, C. G., A. S. Daag, F. G. Delfin Jr., *et al.* (1996). Eruptive history of Mount Pinatubo. *In*: Newhall, C. G. and R. S. Punongbayan (eds) *Fire and Mud*. Seattle: University of Washington and Quezon City: PHIVOLCS, 165−195.

Paladio-Melosantos, M. L. O., R. U. Solidum, W. E. Scott, *et al.* (1996). Tephra falls of the 1991 eruptions of Mount Pinatubo. *In*: Newhall, C. G. and R. S. Punongbayan (eds) *Fire and Mud*. Seattle: University of Washington and Quezon City: PHIVOLCS, 513–535.

Pallister, J. S., R. P. Hoblitt, G. P. Meeker, R. J. Knight and D. F. Siems (1996). Magma mixing at Mount Pinatubo: petrographic and chemical evidence from the 1991 deposits. *In*: Newhall, C. G. and R. S. Punongbayan (eds) *Fire and Mud*. Seattle: University of Washington and Quezon City: PHIVOLCS, 687–731.

Pyle, D. M. (1989). The thickness, volume and grainsize of tephra fall deposits. *Bulletin of Volcanology*, **51**, 1–15.

Rodolfo, K. S., J. V. Umbal, R. A. Alonso, *et al.* (1996). Two years of lahars on the western flanks of Mount Pinatubo: initiation, flow processes, deposits and attendant geomorphic and hydraulic changes. *In*: Newhall, C. G. and R. S. Punongbayan (eds) *Fire and Mud*. Seattle: University of Washington and Quezon City: PHIVOLCS, 989–1013.

Rosi, M., M. L. Paladio-Melosantos, A. Di Muro, R. Leoni and T. Bacolcol (2001). Fall vs flow activity during the 1991 climactic eruption of Pinatubo Volcano (Philippines). *Bulletin of Volcanology*, **62**, 549–566.

Ruaya, J. R. and C. C. Panem (1991). Mt. Natib, Philippines: a geochemical model of a caldera-hosted geothermal system. *Journal of Volcanology and Geothermal Research*, **45**, 255–265.

Scott, W. E., R. P. Hoblitt, R. C. Torres, *et al.* (1996). Pyroclastic flows of the June 15, 1991, climactic eruption of Mount Pinatubo. *In*: Newhall, C. G. and R. S. Punongbayan (eds) *Fire and Mud*. Seattle: University of Washington and Quezon City: PHIVOLCS, 545–570.

Sheridan, M. F. (1979). Emplacement of pyroclastic flows: A review. *In*: Chapin, C. E. and W. E. Elston (eds) *Ash-flow Tuffs*, Geological Society of America Special Paper **180**, 125–136.

Siebert, L. and T. Simkin (2007). Volcanoes of the world: an illustrated catalog of holocene volcanoes and their eruptions. Smithsonian Institution, Global Volcanism Program Digital Information Series, GVP-3. http://www.volcano.si.edu/world/

Sigurdsson, H. and S. Carey (1989). Plinian and co-ignimbrite tephra fall from the 1815 eruption of Tambora volcano. *Bulletin of Volcanology*, **51**, 243–270.

Simkin, T. and L. Siebert (1994). *Volcanoes of the World*. Tucson, AZ: Geoscience Press.

Sparks, R. S. J., M. I. Bursik, S. N. Carey, it et al. (1997). *Volcanic Plumes*. New York: John Wiley & Sons.

Spence, R. J. S., A. Pomonis, P. J. Baxter, it et al. (1996). Building damage caused by the Mount Pinatubo eruption of June 15, 1991. *In*: Newhall, C. G. and R. S. Punongbayan (eds) *Fire and Mud*. Seattle: University of Washington and Quezon City: PHIVOLCS, 1055–1061.

Suzuki, T. (1983). A theoretical model for dispersion of tephra. *In*: Shimozuru, D. and I. Yokoyama (eds) *Arc Volcanism; Physics and Tectonics*. Tokyo: Terra Scientific Publishing, 95–113.

Tahira, M., M. Nomura, Y. Sawada and K. Kamo (1996). Infrasonic and acoustic-gravity waves generated by the Mount Pinatubo Eruption of June 15, 1991. *In*: Newhall, C. G. and R. S. Punongbayan (eds) *Fire and Mud*. Seattle: University of Washington and Quezon City: PHIVOLCS, 601–613.

Todesco, M., A. Neri, T. Esposti Ongaro, *et al.* (2002). Pyroclastic flow hazard assessment at Vesuvius (Italy) by using numerical modeling. I. Large-scale dynamics. *Bulletin of Volcanology*, **64**, 155–177.

van Westen, C. J. and A. S. Daag (2005). Analysing the relation between rainfall characteristics and lahar activity at Mount Pinatubo, Philippines. *Earth Surface Processes and Landforms*, **30**, 1663–1674.

Wiesner, M. G., Y. Wang and L. Zheng (1995). Fallout of volcanic ash to the deep South

China Sea induced by the 1991 eruption of Mount Pinatubo (Philippines). *Geology*, **23**, 885–888.

Wolfe, E. W. and R. P. Hoblitt (1996). Overview of the eruptions. *In*: Newhall, C. G. and R. S. Punongbayan (eds) *Fire and Mud*. Seattle: University of Washington and Quezon City: PHIVOLCS, 3–20.

Wolfe, J. A. and S. Self (1983). Structural lineaments and Neogene volcanism in southwestern Luzon. *In*: Hayes, D. E. (ed) *The Tectonic and Geological Evolution of Southeast Asian Seas and Islands: Part 2*, American Geophysical Union Monograph **27**, 157–172.

Yamakoshi, T., Y. Doi and N. Osanai (2005). Post-eruption hydrology and sediment discharge at the Miyakejima volcano, Japan. *Zeitschrift für Geomorphologie*, **140**, 55–72.